Photodissociation dynamics of carbon suboxide at 193 and 248 nm

D. J. Anderson and R. N. Rosenfeld

Citation: The Journal of Chemical Physics **94**, 7857 (1991); doi: 10.1063/1.460121
View online: http://dx.doi.org/10.1063/1.460121
View Table of Contents: http://scitation.aip.org/content/aip/journal/jcp/94/12?ver=pdfcov
Published by the AIP Publishing

Photodissociation dynamics of carbon suboxide at 193 and 248 nm

D. J. Anderson and R. N. Rosenfeld[a)]
Department of Chemistry, University of California at Davis, Davis, California 95616

(Received 9 October 1990; accepted 13 December 1990)

The nascent CO vibrational, rotational, and translational energies, following the UV photolysis of carbon suboxide at 193 and 248 nm, were determined by time-resolved tunable diode laser infrared absorption spectroscopy. A statistical model for energy disposal fits the experimentally observed vibrational distributions and average translational energies at both photolysis wavelengths. The model fails to account for the experimental rotational distributions that are much "colder" than the model predictions. An impulsive model for dissociation could not account for the observed energy partitioning at both photolysis wavelengths. These results suggest that at 193 nm the primary photoproducts are $CO(X\,^1\Sigma^+)$ and $C_2O(\tilde{a}\,^1\Delta)$, and that at 248 nm the primary photoproducts are $CO(X\,^1\Sigma^+)$ and $C_2O(\tilde{X}\,^3\Sigma^-)$.

I. INTRODUCTION

Molecular photodissociation reactions provide an opportunity to explore, in detail, fundamental questions about chemical reactivity and the forces that control chemical reactions.[1-8] Measurements of product energy distributions and angular orientations can be compared to predictions made with various simple, limiting case,[9-14] or more elaborate physical models.[15-23] These comparisons can provide insight into the geometry of the dissociating species and the potential energy surfaces involved. Theoretical models for half-collision events, i.e., photodissociation processes, have seen much success.[24] The photodissociation dynamics of small molecules are becoming increasingly well understood.[5] Systems of four or fewer atoms are often amenable to complete experimental characterization.[6] By using laser and molecular beam methods, it is often possible to prepare single rovibronic states of a reactant, and to completely characterize the product quantum state distributions.[25,26] For sufficiently simple systems, accurate potential energy surfaces can be calculated[27] or determined experimentally.[28] The dissociation reactions on these surfaces can often be investigated using quantum mechanical models[29] and classical or semiclassical trajectory methods.[30] The investigation of larger polyatomic systems presents some problems. Excitation of a single rovibronic reactant state is not always possible. In these cases, only the initial energy rather than the initial quantum state can be specified. Similarly, the assignment of complete product quantum state distributions may not be possible. Calculation of potential surfaces by state of the art quantum mechanical models is time consuming and subject to errors for large polyatomic molecules. Despite these difficulties, progress has been made in the study of large molecule dissociation dynamics. Particularly noteworthy examples include the work of Moore and co-workers[31] who have studied the photodissociation of ketene, CH_2CO, and Wittig and co-workers[32,33] who have studied NCNO and $(CH_3)_3CNO$ photodissociation. We have recently developed a model to account for energy disposal in the photodissociation of $W(CO)_6$.[34,35] In these instances, the development of physical models for energy partitioning facilitated the interpretation of the observed product quantum state distributions.

Here, we present a detailed study of the photodissociation dynamics of carbon suboxide. Carbon suboxide provides an interesting test case in the development of models for dissociation dynamics because it may represent an intermediate point between the small and large molecule limits; a linear polyatomic molecule dissociating to a linear triatomic molecule and a diatomic molecule. In this paper we report data on the energy disposal to the carbon monoxide fragment's vibrational, rotational, and translational degrees of freedom following excimer laser photolysis of carbon suboxide at 193 and 248 nm.

The UV photolysis of carbon suboxide can proceed by the pathways shown below:[36]

$$C_3O_2 \rightarrow C_2O(\tilde{X}\,^3\Sigma^-) + CO(X\,^1\Sigma^+), \quad \Delta H^0 \sim 86 \text{ kcal/mol},^{37,38} \tag{1a}$$

$$C_3O_2 \rightarrow C_2O(\tilde{a}\,^1\Delta) CO(X\,^1\Sigma^+), \quad \Delta H^0 \sim 106 \text{ kcal/mol},^{38} \tag{1b}$$

$$C_3O_2 \rightarrow C_2O(\tilde{A}\,^3\Pi_i) + CO(X\,^1\Sigma^+), \quad \Delta H^0 \sim 119 \text{ kcal/mol},^{38} \tag{1c}$$

$$C_3O_2 \rightarrow C_2O(\tilde{b}\,^1\Sigma^+) + CO(X\,^1\Sigma^+), \quad \Delta H^0 \sim 122 \text{ kcal/mol},^{38} \tag{1d}$$

$$C_3O_2 \rightarrow C(^3P) + 2CO(X\,^1\Sigma^+), \quad \Delta H^0 \sim 138 \text{ kcal/mol}.^{36} \tag{2}$$

At wavelengths below ~ 270 nm the production of electronically excited C_2O becomes energetically possible. At 193 nm all five channels are thermochemically accessible, however, channel 2 has been found to have a relative yield of $< 6\%$.[39] Therefore the production of C_2O and CO is the major chan-

[a)] Present address: tbd analysis, inc., 2261 Federal Ave., Los Angeles, CA 90064.

nel, and at this wavelength all three excited electronic states of C_2O are energetically accessible. At 248 nm only channels 1a and 1b are energetically accessible. The UV photolysis of carbon suboxide has received much attention in the past.[40–51] A particularly interesting feature of th is system is that carbon suboxide is a ground state singlet whereas C_2O is a ground state triplet. Therefore channels 1a and 1c should be forbidden based upon spin conservation. However, despite the amount of work done on the UV photolysis of carbon suboxide, there remains considerable uncertainty concerning the primary photoproducts, and their electronic states.

C_2O was first observed by Jacox *et al.*[40] who photolyzed carbon suboxide in an Ar matrix at 4.2 K. The three fundamental infrared bands and an absorption continuum beginning near 500 nm were observed. Devillers and Ramsay[41] obtained well-resolved gas-phase absorption spectra for the $C_2O(\tilde{A}\,^3\Pi_i - \tilde{X}\,^3\Sigma^-)$ transition following flash photolysis of carbon suboxide. The vibrational structure obtained by Devillers and Ramsay corroborated the matrix assignments of Jacox *et al.* Bayes[42,43] has photolyzed mixtures of ethylene and carbon suboxide at 250 and 300 nm. The formation of allene by the reaction of C_2O and ethylene was quenched by triplet scavengers at 300 nm, but not at 250 nm. Bayes concluded that at 250 nm C_2O is produced in the singlet $\tilde{a}^2\Delta$ electronic state, and at 300 nm C_2O is produced in the triplet $\tilde{X}\,^3\Sigma^-$ ground state. Donnelly *et al.*[44] and Pitts *et al.*[45,46] photolyzed carbon suboxide at 266 nm, and used laser-induced fluorescence (LIF) on the $C_2O(\tilde{A}–\tilde{X})$ transition to investigate the ground state $C_2O(\tilde{X}\,^3\Sigma^-)$ generated. Upon searching other spectral regions from 640 to 740 nm, Pitts *et al.*[45] did not detect any excited states of C_2O in contrast with the results of Bayes.[47] Additionally, Becker *et al.*[48] generated C_2O by the 248 nm photolysis of carbon suboxide and found that the $C_2O(\tilde{A}–\tilde{X})$ LIF spectrum that they obtained was almost identical to that of Pitts *et al.*, obtained at 266 nm.[45,46] Bauer *et al.*[49] photolyzed carbon suboxide at 193 nm and monitored the $C_2O(\tilde{A}–\tilde{X})$ emission that grew in over a time period of 5–10 μs. The delay in emission was postulated to be due to a triplet precursor of carbon suboxide or a slow singlet to triplet conversion in C_2O. Yamada *et al.*[50] used infrared absorption spectroscopy to probe the $\tilde{X}\,^3\Sigma^-$ state of C_2O generated by the 193 nm photolysis of carbon suboxide. They observed a slow appearance time of 50 to 100 μs for the formation of $C_2O(\tilde{X}\,^3\Sigma^-)$. Weiner *et al.*[51] used infrared absorption spectroscopy to observe the CO product vibrational energy distribution following photolysis of carbon suboxide at 193 and 248 nm. They saw a detector limited (< 100 ns) appearance of CO at both wavelengths. This effectively eliminates the possibility of a long lived intermediate state of

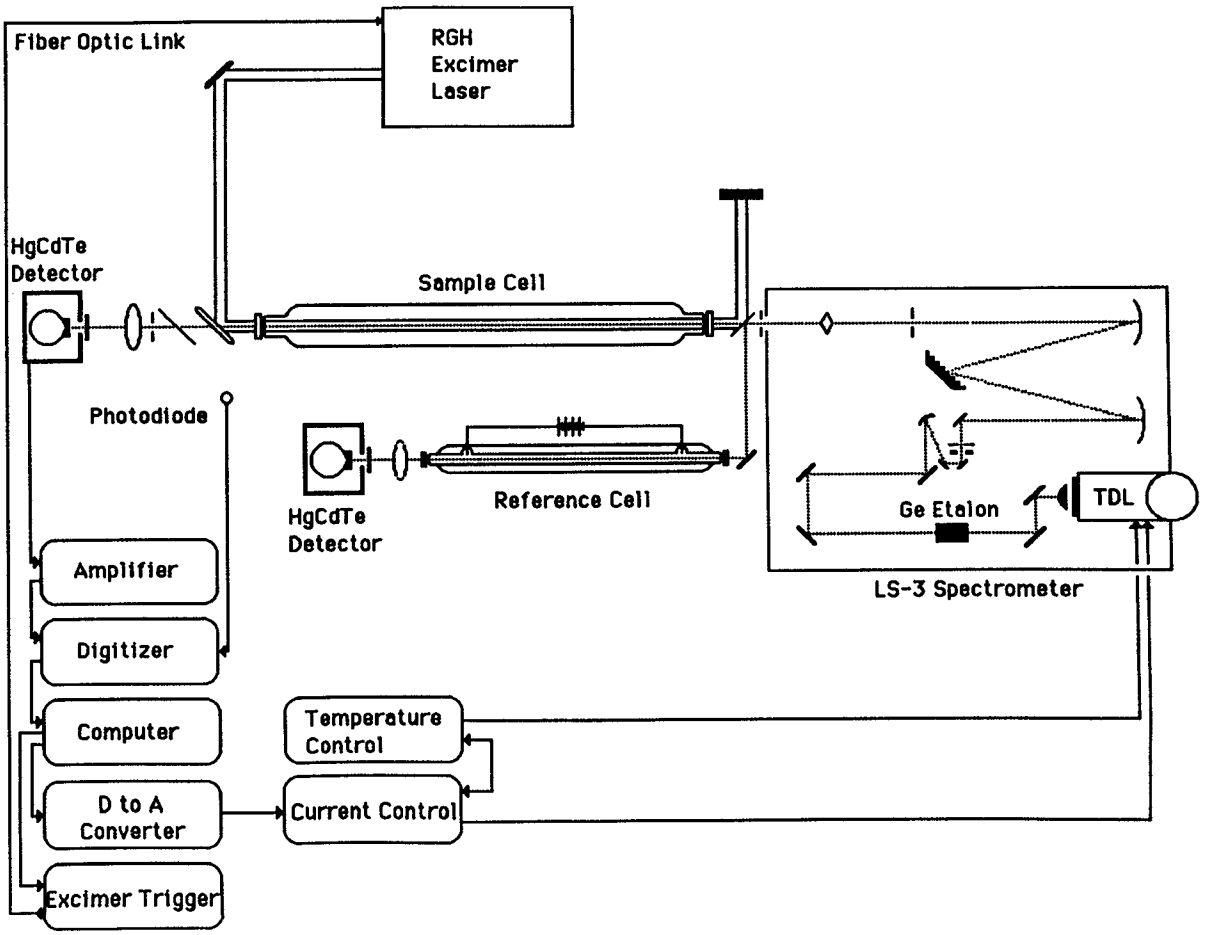

FIG. 1. Instrumentation used to record time-resolved infrared absorption spectra of CO following UV photolysis of C_3O_2.

carbon suboxide, and suggests that an unobserved state of C_2O, possibly a singlet state, is the direct product from the 193 nm photolysis of carbon suboxide.

It is apparent that the primary photochemistry of carbon suboxide is not well understood. We have used high resolution infrared absorption spectroscopy to monitor the vibrational, rotational, and translational energy distributions of the CO product following photolysis of carbon suboxide at 193 and 248 nm. This information is evaluated using a model for energy partitioning in the dissociation of carbon suboxide to investigate the photodissociation dynamics of carbon suboxide.

II. EXPERIMENTAL

The instrumentation used in our experiment is shown in Fig. 1. C_3O_2 (0.025–0.100 Torr) was introduced into a 1.41 m Pyrex sample cell (background pressure $\leqslant 10^{-4}$ Torr) fitted with vacuum ultraviolet grade CaF_2 windows. Sample pressures were measured with a capacitance manometer (MKS Baratron 223B, 0–1 Torr). The photolysis of C_3O_2 was accomplished using a pulsed rare gas–halide excimer laser (Lambda Physik EMG-101) operating at either 193 nm (ArF*) or 248 nm (KrF*). UV fluences were kept within 1–6 mJ/cm^2 (193 nm) and 1–33 mJ/cm^2 (248 nm) to minimize multiphoton absorption processes. Production of CO in specific rovibrational states was monitored using the output from a tunable diode laser (TDL) system (Laser Analytics LS-3). A MBE diode (Laser Photonics) was used which operated in the range 1980–2200 cm^{-1}, providing semicontinuous coverage of the infrared transitions of CO. The output of the diode laser, after passing through the mode isolation monochromator, was collimated with a 1.27 cm diam $f/10.0$ CaF_2 lens and directed through the sample cell. A portion of the beam (ca. 5%) was directed through a 50 cm long water cooled dc discharge reference cell. Absolute frequency calibration of the TDL was accomplished using reference gases (e.g., ^{12}CO, ^{13}CO, OCS),[52] and a 1 in. solid Ge etalon with a free spectral range of ca. 0.0469 cm^{-1}. The discharge cell was used to determine the frequency positions of vibrationally excited CO molecules. Using these references, it was possible to bring the TDL frequency into resonance with any desired CO rovibrational transition. Since the TDL linewidth ($\sim 10^{-4}$ cm^{-1}) is 50–100 times smaller than the Doppler limited width of the infrared transitions of interest, care was taken to maintain the TDL output frequency at line center. High resolution tuning of the TDL frequency was accomplished by varying the injection current.

Transient absorption of the infrared probe beam following UV excitation of C_3O_2 was followed using a liquid N_2 cooled HgCdTe detector (Infrared Associates, active area 0.5 mm$\times$0.5 mm, $\tau = 177$ ns). The signals from the detector were amplified, digitized (LeCroy TR8837, 32 MHz), accumulated, and averaged in order to obtain good signal to noise levels (i.e., $S/N \geqslant 10$). The signals were normalized with respect to the average infrared and UV powers, measured before and after each transient.

Experiments were performed in two ways. For experiments that measured vibrational and rotational state populations, the TDL frequency was tuned to and maintained at line center during the course of the experiment. Static fills of C_3O_2 either neat or with added He or H_2 buffer gas were used. The sample was changed after each time-resolved infrared absorption signal was averaged, minimizing effects due to photolysis products and depletion of the sample. For experiments that measured Doppler profiles, the TDL frequency was stepped across the CO absorption line as data were collected. This was accomplished by using a computer controlled digital to analog converter (DAC) to step the TDL injection current after each transient had been averaged and stored. The DAC had a 0–1 V range and 12 bit resolution. For the diode employed in these experiments the minimum frequency shift that could be obtained with the DAC was 9×10^{-5} cm^{-1} ($\sim$2% of the Doppler broadened FWHM). Typically, frequency shifts of 3.6×10^{-4} cm^{-1} were obtained, resulting in approximately 30–35 points obtained per Doppler profile. Flowing samples of C_3O_2 and low UV pulse rates (ca. 1–2 Hz) were used to minimize effects due to sample degradation.

For all experiments performed, the UV and IR beams were counter propagated collinearly through the sample cell. The UV beam diameter was $\sim$1.0 cm and the IR beam was $\sim$0.5 cm. The UV beam had a uniform flux across the beam diameter. The input into the HgCdTe detector was filtered with an IR bandpass filter to remove any stray UV or visible light. The detectors and their associated preamplifiers were shielded from electromagnetic interference by enclosing them in grounded aluminum boxes.

C_3O_2 was prepared by the dehydration of malonic acid, according to the procedure of Long *et al.*[53] Purification was accomplished using the procedure of Miller *et al.*[54] Purity was checked by infrared absorption spectroscopy and mass spectrometry.

III. RESULTS

A. 193 nm photodissociation

The photoexcitation of C_3O_2 at 193 nm results in the production of C_2O and CO as the major primary photoproducts ($\geqslant$94%).[39] We have characterized the CO photofragment vibrational and rotational distributions, and average translational energy, by infrared transient absorption spectroscopy.

The nascent CO vibrational energy distribution was determined by monitoring the transient absorption of infrared radiation resonant with line center of the CO $P_{v',v''}(4)$ transition of each vibrational level ($v'' = 0 - 4$). The rotational distributions in each vibrational level were thermalized with 5 Torr of added He or H_2 buffer gas. The peak absorbance amplitudes were used to calculate the vibrational distribution. Under the experimental conditions used, CO vibrational relaxation occurs slowly,[55–57] permitting the nascent vibrational distribution to be measured. The measured CO vibrational distribution did not vary significantly when measured at delay times from 1 to 4 μs. We find relative CO vibrational populations, $N_0/N_1/N_2/N_3/N_4 = 1.00/0.37/0.17/0.062/0.015$. We obtained essentially identical populations using either He or H_2 as the buffer gas. When these

relative vibrational state populations were fit to a Boltzmann distribution (Fig. 2), the slope of the best straight line defined an effective nascent CO vibrational temperature, $T_v^0 = 3030 \pm 49$ K. Here, T_v^0 is not a true thermodynamic temperature due to energy restrictions on the maximum CO vibrational state that can be populated in the photodissociation reaction. In our experiment CO($v > 4$) is not observed due to signal to noise limitations, and TDL frequency coverage limitations. The highest vibrational levels of CO that can be populated by the 193 nm photolysis of carbon suboxide are $v = 10$, 6, 4, and 3, corresponding to channels 1a–1d, respectively.

The rotational state distributions for CO($v = 0$), CO($v = 1$), and CO($v = 2$) were obtained by monitoring the transient absorption of infrared radiation resonant with line center of the CO $P_{v',v''}(J)$ transitions. Not all rotational transitions were monitored due to a lack of stable TDL modes at the appropriate frequencies. Data were obtained for CO $P_{v',v''}$ (1 — 30). C_3O_2 pressures were kept as low as possible (0.050–0.100 Torr) to reduce the rate of collisional relaxation.[58]

An effective rotational temperature, T_r, was defined by fitting the measured distributions to a Boltzmann distribution function as shown in Fig. 3. At the pressures used in our experiments, collisional relaxation may occur on a time scale approaching our detection system rise time. Therefore, nascent rotational distributions cannot be obtained directly from the transient absorption data. However, the nascent

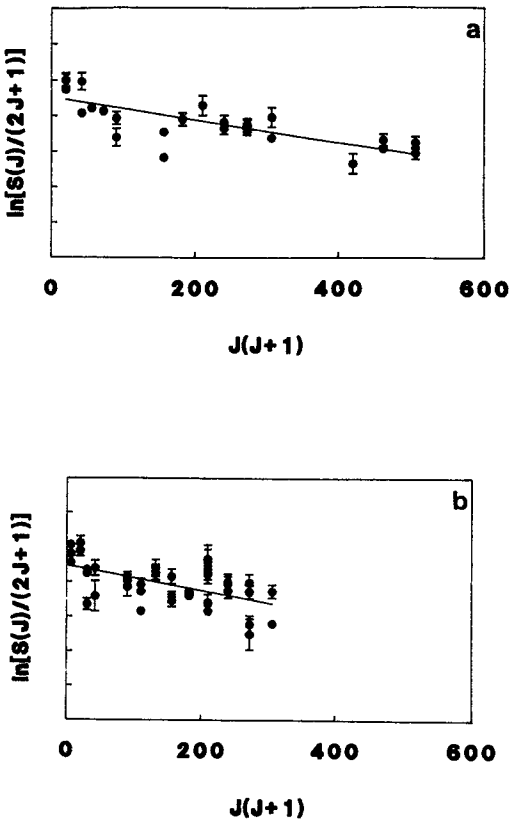

FIG. 3. CO rotational distributions. (a) CO($v = 0$) rotational distribution obtained 2.0 μs after the 193 nm photolysis of 50 mTorr of C_3O_2; (b) CO($v = 1$) rotational distribution obtained 2.0 μs after the 193 nm photolysis of 100 mTorr of C_3O_2. The best fit lines correspond to effective CO rotational temperatures of 920 $\pm$ 63 K and 556 $\pm$ 30 K, respectively.

rotational distributions can be estimated by extrapolation of T_r to time $t = 0$ (corresponding to 0 collisions). A plot of T_r versus time (or equivalently, number of collisions) following the UV photolysis of C_3O_2 is shown in Fig. 4. We believe that the early time behavior of T_r is due to two factors. Firstly, the initial decrease in T_r is due to translational cooling of the observed rotational distribution. Initially, due to energy constraints, low J states have higher translational energies

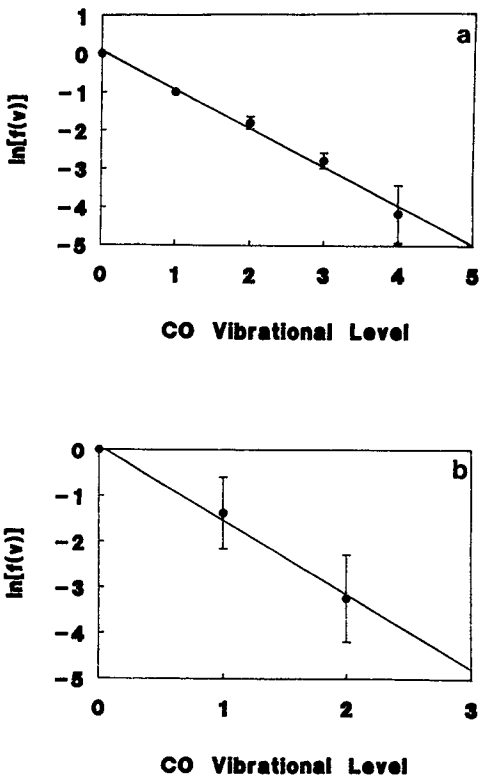

FIG. 2. CO vibrational distribution following the UV photolysis of C_3O_2. C_3O_2 pressure = 50 mTorr, He buffer gas pressure = 5 Torr, distribution measured at 3.0 μs delay following the photolysis pulse. (a) Photolysis wavelength = 193 nm; (b) photolysis wavelength = 248 nm.

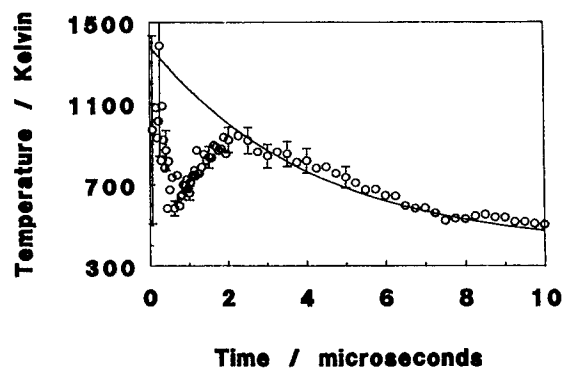

FIG. 4. The CO($v = 0$) rotational distribution as a function of time after the 193 nm photolysis of 50 mTorr of C_3O_2. The line is an exponential fit to the data at times $t > 2.0$ μs, and extrapolates to an estimated nascent CO($v = 0$) rotational temperature, $T_r^0 = 1380 \pm 99$ K.

than high J states, which results in larger Doppler widths and smaller line center absorption amplitudes for the low CO J states. This effect results in the observed rotational distribution being "hotter" than the actual distribution. As collisions thermalize the translational energy of the products, this effect is diminished, and the observed rotational distribution cools. Indeed, the initial decrease in T_r approximately parallels the relaxation of the CO translational energy (*vide infra*). Secondly, the increase in T_r at intermediate times, 1 to 2 μs, is due to a significant upper vibrational state population that has a characteristic rotational distribution that is "cooler" than the rotational distribution of the lower state. This serves to decrease the absorption amplitude of the lower J states with respect to the higher J states. This behavior is most pronounced for the observed rotational distribution in $v = 0$, and less pronounced for $v = 1,2$. An exponential extrapolation of T_r to time $t = 0$, using $T_r(t \geqslant 2\ \mu s)$, yields estimated nascent rotational temperatures of: $T_r^0(v = 0) = 1380 \pm 99$ K, $T_r^0(v = 1) = 1040 \pm 38$ K, and $T_r^0(v = 2) = 751 \pm 100$ K.

The translational energy of the CO(v,J) product was investigated by time-resolved measurements of the absorption line shape. At the pressures used in our experiments, Doppler broadening is the major source of line broadening.[59] The Doppler broadened line shapes for various CO P and R branch transitions were determined by measuring the transient absorption of infrared radiation at 0.0003 to 0.00015 cm^{-1} increments across the absorption line. Computer control of the data collection and archiving, excimer triggering, and TDL injection current greatly enhanced the collection of line shape data, allowing from 30 to 60 averaged transients to be obtained across a single absorption line.

In fitting the experimental line shapes, we assumed an isotropic Maxwellian distribution of kinetic energy. Indeed, the experimental data were well fit by a Gaussian function describing the Doppler broadening of an absorption line [Eq. (3)],

$$I(\tilde{\nu}) = K \exp[-(\tilde{\nu} - \tilde{\nu}_0)^2/\sigma_d^2], \quad (3)$$

where $\tilde{\nu}_0$ is the line center frequency, $\tilde{\nu}$ is the absolute frequency, σ_d is the Doppler broadened full width at half-maximum (FWHM), and K is a proportionality constant. The FWHM is related to the translational temperature by Eq. (4), where c is the speed of light, M is the molecular weight of CO, and R is the ideal gas constant:

$$T_t = [c^2\sigma_d^2 M/\tilde{\nu}_0^2 8R \ln 2]. \quad (4)$$

The experimental data for several absorption lines and the corresponding best fit Gaussians are shown in Fig. 5. From the fit of the data we were able to derive an effective translational temperature, T_t. The relaxation of T_t with time (or equivalently, number of collisions) following the photodissociation event is shown in Fig. 6. The nascent translational temperature, T_t^0, for CO(v,J), was determined by an exponential extrapolation of the T_t data to time $t = 0$, corresponding to 0 collisions. The nascent translational temperatures so determined are given in Table I.

B. 248 nm photodissociation

The photoexcitation of C_3O_2 at 248 nm results in the production of C_2O and CO as the primary photoproducts.

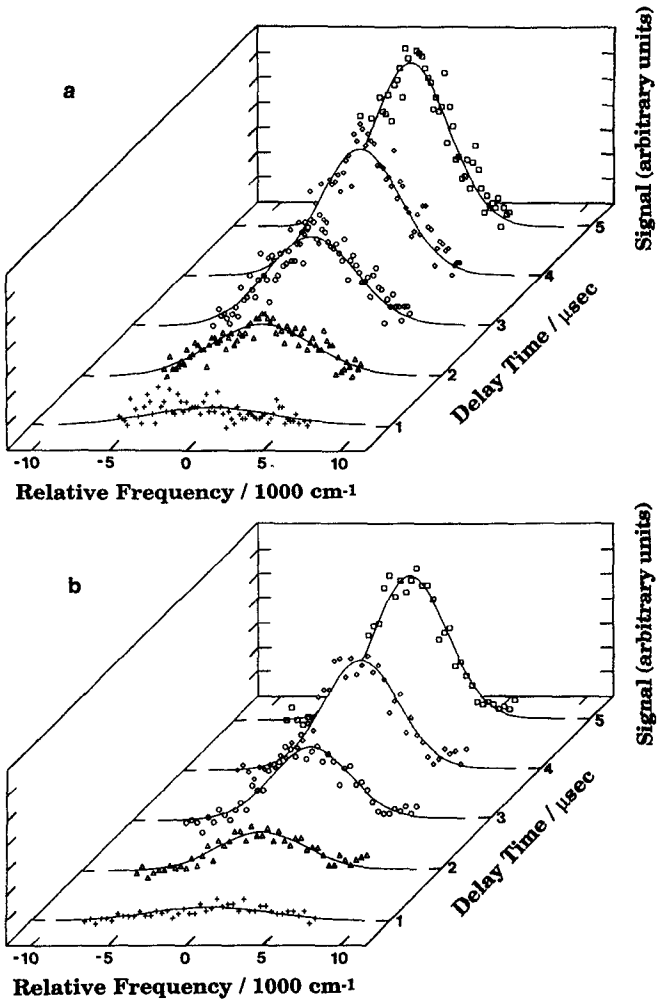

FIG. 5. Doppler line shapes for CO($v = 0,1$). (a) CO $P_1(8)$ absorption line shape obtained after the 193 nm photolysis of 85.5 mTorr of C_3O_2; (b) CO$P_2(4)$ absorption line shape obtained after the 193 nm photolysis of 100 mTorr of C_3O_2.

The CO vibrational and rotational distributions, and average translational energy were determined in the same way as described above.

The nascent CO vibrational energy distribution was determined by observing both the $P_{v',v''}(4)$ and $P_{v',v''}(12)$ tran-

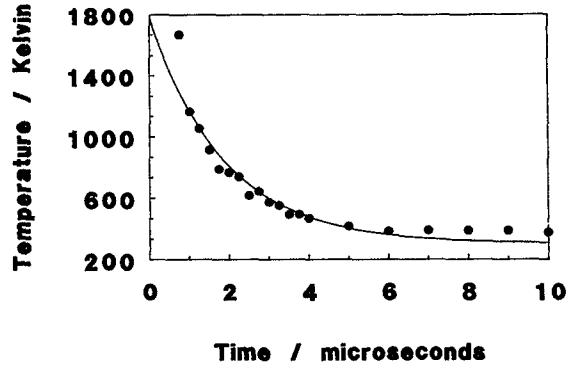

FIG. 6. Translational temperature of CO($v = 0$, $J = 8$) after the 193 nm photolysis of 50 mTorr of C_3O_2. The line is an exponential extrapolation to time $t = 0$, yielding an estimated nascent translational temperature, $T_t^0(v = 0,\ J = 8) = 1740 \pm 290$ K.

TABLE I. Translational energy disposal to CO in the UV photodissociation of C_3O_2.

CO rovibrational state (v,J)	Photolysis wavelength, (nm)	Translational temperature (K)
(0,8)	193	1740 ± 290
(0,16)	193	1389 ± 147
(0,26)	193	729 ± 159
(1,4)	193	1400 ± 410
(2,3)	193	1100 ± 349
(0, 8)	248	1300 ± 232
(1, 4)	248	1092 ± 130

sition of each vibrational level ($v'' = 0 - 2$). We find relative CO vibrational populations of: $N_0/N_1/N_2 = 1.00/0.277/0.049$. Again, these relative populations were invariant with the type of buffer gas used (He, H_2), and the delay time from 1 to 4 μs. The fit of the vibrational level populations to a Boltzmann distribution (Fig. 2) yields a nascent CO vibrational temperature, $T_v^0 = 2070 \pm 22$ K. For carbon suboxide photolysis at 248 nm, the highest CO vibrational levels that can be populated are $v = 4$ and $v = 1$, corresponding to channels 1a and 1b, respectively.

The rotational energy distributions for CO($v = 0$) and CO($v = 1$) were determined from the line center absorption amplitudes of the $P_{v',v''}(J)$ rovibrational transitions ($v'' = 0,1$; $J = 1 - 30$). The nascent rotational temperatures were determined by fitting the rotational distributions to a Boltzmann distribution (Fig. 3) and extrapolating the effective rotational temperature to time $t = 0$ (Fig. 4). We obtained estimated nascent rotational temperatures: T_r^0 ($v = 0$) $= 1800 \pm 480$ K and $T_r^0(v = 1) = 1000 \pm 59$ K. At this photolysis wavelength, the observed rotational distributions did not exhibit a rotational bias due to upper vibrational state populations. This result is consistent with the smaller upper CO vibrational level populations observed at this photolysis wavelength. However, we do see an initial rapid cooling of the observed rotational distribution which we attribute to translational cooling within the observed vibrational level.

The CO translational energy was measured for several CO rovibrational states. The line shapes obtained were fit to Gaussian functions as described above, and the effective translational temperatures obtained were exponentially extrapolated to time $t = 0$ to obtain estimated nascent translational temperatures, T_t^0 (Figs. 5 and 6). The nascent translational temperatures obtained are given in Table I.

IV. DISCUSSION

When carbon suboxide is irradiated at 193 or 248 nm the primary photoprocess is dissociation to C_2O and CO. However, there is much uncertainty about the electronic states of carbon suboxide and C_2O that are involved in the dissociation process. The most recent investigation into the UV absorption spectra of carbon suboxide was performed by Roebber who made the following assignments.[60] When irradiated at 193 nm, carbon suboxide can undergo a $\pi \rightarrow \pi^*$ transition to the degenerate $^1\Sigma_g^-$ and $^1\Delta_g$ states, or a $\pi \rightarrow \sigma$ transition to the $^1\Pi_u$ state. At 248 nm, carbon suboxide absorbs a photon and undergoes a $\pi \rightarrow \pi^*$ transition to the degenerate $^1\Sigma_u^-$ and $^1\Delta_u$ states. The correlation of carbon suboxide states with CO and C_2O states has been worked out by Minato *et al.*[61] for the dissociation of carbon suboxide by either a linear or bent geometry. The carbon suboxide states initially populated at 193 nm: $^1\Sigma_g^-$, $^1\Delta_g$, and $^1\Pi_u$, do not correlate with any energetically accessible product states for either dissociation geometry. Carbon suboxide has a very large rovibrational state density in its ground electronic state, due to a very low frequency bending mode ($\nu_7 \approx 20\ \mathrm{cm}^{-1}$).[62] It is known that molecules with large rovibrational state densities can undergo rapid radiationless transitions to lower electronic states prior to dissociation.[63] We therefore postulate that carbon suboxide that is photoexcited at 193 nm must initially undergo a radiationless transition to the ground or other low-lying electronic state prior to dissociation. Ground state carbon suboxide, $\tilde{X}\,^1\Sigma_g^+$, correlates with $C_2O(\tilde{b}\,^1\Sigma^+)$ for a linear dissociation geometry, and with $C_2O(\tilde{a}^1\Delta)$ for a nonlinear dissociation geometry. The carbon suboxide $^1\Delta_u$ state initially populated at 248 nm correlates with $C_2O(\tilde{a}^1\Delta)$ and with $C_2O(\tilde{b}\,^1\Sigma^+)$ for linear and nonlinear dissociations, respectively. The $^1\Sigma_u^-$ state of carbon suboxide correlates with $C_2O(\tilde{a}^1\Delta)$ for a nonlinear dissociation, but does not correlate with any energetically accessible C_2O states for a linear dissociation. The involvement of any of the above discussed electronic states in the dissociation of carbon suboxide may be determined by comparing the observed CO product energy distributions to some physical models for energy partitioning.

Statistical models have proven useful in calculating product energy distributions for photodissociation reactions. Statistical or phase space models predict the probability of forming products in a particular set of quantum states by determining the corresponding volume of available phase space. In the standard formulation of phase space theory,[15] the available volume of phase space corresponding to a particular reaction channel is constrained by conservation of angular momentum and total available energy. We have used an alternate formulation of phase space theory, which we call "microcanonical" phase space theory, to predict the product energy distributions from the dissociation of polyatomic molecules.[34,35] The microcanonical model calculates the available phase space volumes under the constraint of conservation of total energy only, i.e., angular momentum constraints are ignored.[64,65] It has been shown that statistical or phase space models best describe reactions that have no energy barrier to dissociation other than the endothermicity of the reaction.[66] For example, the ground state dissociations of CH_2CO and NCNO proceed without appreciable barriers in excess of the endothermicity of the reaction.[32,33] These systems are well described by statistical phase space models. The dissociation of H_2CO to H_2 and CO proceeds across a substantial barrier (in excess of the endothermicity) to dissociation.[67] Indeed, the observed product distributions following the photodissociation of formaldehyde are markedly nonstatistical.[68] The dissociation of carbon suboxide

to C_2O and CO is thought to proceed without a significant barrier. Evidence to support this comes from the work of Jacox *et al.*[40] who observed C_2O recombine with CO in a cryogenic matrix to form carbon suboxide, indicating the lack of a substantial barrier. We therefore expect that a statistical model may successfully describe the dissociation dynamics of carbon suboxide.

The microcanonical model used to calculate the CO product energy distributions from the photodissociation of carbon suboxide is described below. The probability of forming CO in a given vibrational state v, rotational state J, with a translational energy E_t, given a total available energy, $E = h\nu - DH^0$, to be partitioned among the products is given by $f_{CO}(v,J,E_t;E)$ in Eq. (5):

$$f_{CO}(v,J,E_t;E) = (2J+1)P_{CCO}(E - E_e - E_v - E_J - E_t - E_t')\sqrt{E_t + E_t'}, \quad (5)$$

where $P_{CCO}(E^\dagger)$ is the number of C_2O rovibrational states at energy $E^\dagger$, E_e is the C_2O electronic term energy, E_v and E_J are the CO vibrational and rotational energies, and E_t' is the C_2O center of mass kinetic energy. From the conservation of linear momentum, Eq. (5) can be rewritten as given in Eq. (6), where $M = 1 + (m_{CO}/m_{CCO}) = 1.7$:

$$f_{CO}(v,J,E_t;E) = (2J+1)P_{CCO}(E - E_e - E_v - E_J - ME_t)\sqrt{ME_t}. \quad (6)$$

The average kinetic energy of a CO molecule formed in a specific rovibrational state (v,J), is then given by Eq. 7, where the limits on E_t are given by: $E_{t;\min} = 0$, and $E_{t;\max} = (E - E_e - E_v - E_J)/M$. The probabilities of forming CO is a specific rovibrational state, and in a specific vibrational state are then given by Eqs. (8) and (9):

$$\langle E_t(v,J;E)\rangle = \frac{\int_{E_t;\min}^{E_t;\max} f_{CO}(v,J,E_t;E)E_t\,dE_t}{\int_{E_t;\min}^{E_t;\max} f_{CO}(v,J,E_t;E)dE_t}, \quad (7)$$

$$f_{CO}(v,J;E) = \frac{\int_{E_t;\min}^{E_t;\max} f_{CO}(v,J,E_t;E)dE_t}{\sum_{v=0}^{v_{\max}}\sum_{J=0}^{J_{\max}}\int_{E_t;\min}^{E_t;\max} f_{CO}(v,J,E_t;E)dE_t}, \quad (8)$$

$$f_{CO}(v;E) = \frac{\sum_{J=0}^{J_{\max}}\int_{E_t;\min}^{E_t;\max} f_{CO}(v,J,E_t;E)dE_t}{\sum_{v=0}^{v_{\max}}\sum_{J=0}^{J_{\max}}\int_{E_t;\min}^{E_t;\max} f_{CO}(v,J,E_t;E)dE_t}. \quad (9)$$

Equations (5)–(9) were evaluated using a direct count algorithm to compute the value of $P_{CCO}(E^\dagger)$. The C_2O rotational constants and vibrational frequencies used were those of Devillers and Ramsay.[41] The integrals in Eq. (7)–(9) were calculated to a convergence of better than 10^{-3}. The results of the calculations for the photodissociation of carbon suboxide at 193 and 248 nm are given in Tables II and III. The calculations were performed for various electronic states of C_2O as possible products.

The results of the calculations for the photodissociation

TABLE II. Energy disposal to CO in the 193 nm photodissociation of C_3O_2.

Relative vibrational state populations				
		Microcanonical model		
CO vibrational level, v	Experiment	1[a]	2[b]	3[c]
0	1.00 ± 0	1.00	1.00	1.00
1	0.37 ± 0.05	0.51	0.37	0.26
2	0.17 ± 0.03	0.25	0.12	0.045
3	0.062 ± 0.013	0.12	0.031	0.005
4	0.015 ± 0.012	0.051	0.006	10^{-4}
Effective temperatures (K)				
		Microcanonical model		
	Experiment	1[a]	2[b]	3[c]
Vibrational	3030 ± 49	4238	2547	1518
Rotational				
$v=0$	1380 ± 99	4907	3565	2613
$v=1$	1040 ± 38	4556	2796	2165
$v=2$	751 ± 100	4247	2629	1624
Translational				
$v=0, J=8$	1740 ± 290	2767	1950	1423
$v=0, J=16$	1389 ± 147	2720	1883	1374
$v=0, J=26$	729 ± 159	2630	1740	1272
$v=1, J=4$	1400 ± 410	2543	1605	1168
$v=2, J=2$	1100 ± 349	2326	1449	884

[a] Calculated for $C_2O(\tilde{X}\,^3\Sigma^-)$.
[b] Calculated for $C_2O(\tilde{a}\,^1\Delta)$.
[c] Calculated for $C_2O(\tilde{A}\,^3\Pi,)$.

TABLE III. Energy disposal to CO in the 248 nm photodissociation of C_3O_2.

Relative vibrational state populations			
		Microcanonical model	
CO vibrational level, v	Experiment	1[a]	2[b]
0	1.00 ± 0	1.00	1.00
1	0.277 ± 0.144	0.262	2×10^{-5}
2	0.049 ± 0.015	0.049	
Effective temperatures (K)			
		Microcanonical model	
	Experiment	1[a]	2[b]
Vibrational	2070 ± 22	2080	286
Rotational			
$v=0$	1800 ± 480	2648	855
$v=1$	1000 ± 59	2202	
Translational			
$v=0, J=8$	1300 ± 242	1452	414
$v=1, J=4$	1092 ± 130	1194	

[a] Calculated for $C_2O(\tilde{X}\,^3\Sigma^-)$.
[b] Calculated for $C_2O(\tilde{a}\,^1\Delta)$.

of carbon suboxide at 193 nm indicate that less than the full available energy, $h\nu$-DH^0, is available to the CO fragment (see Table II, column 1). If we assume that C_2O is formed in an excited electronic state, the energy available to the dissociating molecule can be reduced. We have done this for C_2O formed in the $\tilde{a}^1\Delta$, and $\tilde{A}^3\Pi_i$ electronic states. In doing so, we have assumed that there is no additional barrier beyond the electronic term energy of the C_2O fragment. The results for $C_2O(\tilde{a}^1\Delta)$ compare reasonably well with the experimentally observed distributions for the CO vibrational and translational degrees of freedom. The experimentally estimated nascent CO rotational distributions however, are substantially "colder" than the predicted distributions.

The observed rotational distributions exhibit a temporal behavior due to translational and rotational aliasing of the actual rotational distributions. The translational aliasing of the rotational distribution occurs because, in the nascent CO product, low J states within a given vibrational level have larger FWHMs (and consequently smaller line center amplitudes) than the high J states. We have calculated that the error in the observed rotational distribution due to this translational line broadening effect will result in an overestimate of the rotational temperature by ca. 15%–20%. The observed rotational distributions do exhibit an initial rapid decrease in T_r that we attribute to translational cooling. Rotational aliasing of the observed rotational distribution is caused by the population of upper CO vibrational levels. Since absorption spectroscopy measures the difference in population between two levels, the population in the upper state reduces the absorption signal. We have used a simple two-level model to simulate the effects of having a significant upper vibrational state population upon the observed rotational distribution in the lower state.[69] The results of this model are shown in Fig. 7. The initial vibrational populations used were the experimentally measured values for $v = 0$ and $v = 1$. The rotational distribution in each level was initially characterized by either the estimated nascent rotational temperature, or the theoretically predicted distributions. The theoretically observed rotational distribution for the lower level was determined from the differences in the upper and lower levels for all the possible P branch transitions. The temporal behavior was determined by relaxing the rotational distribution within each level according to the experimentally measured relaxation rate. While the actual rotational distributions relax with exponentially decreasing characteristic temperatures, the observed rotational distribution initially shows an increase in effective rotational temperature. In light of these effects, we have used only the later time ($t \geqslant 2\,\mu$s) data to fit the relaxation of the observed rotational distributions.

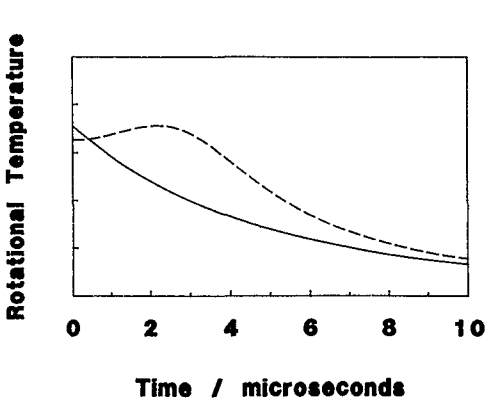

FIG. 7. Model of rotational aliasing of a rotational distribution. The solid line is the temperature of the actual rotational distribution in $CO(v = 0)$. The dashed line is what the observed rotational temperature would look like given a significant upper vibrational state population.

The results of the microcanonical calculation for the photodissociation of carbon suboxide at 248 nm are in good agreement with the experimentally measured CO vibrational and translational distributions, for C_2O formed in the $\tilde{X}^3\Sigma^-$ ground electronic state. However, as in the 193 nm photolysis, the experimentally measured rotational distributions are considerably "colder" than the predicted distributions. The rotational distributions exhibit an initial rapid decrease in effective temperature, T_r, due to the translational aliasing effect. However, the effects due to rotational aliasing were not seen at this photolysis wavelength. This result is consistent with the "cooler" vibrational distribution observed for 248 nm photolysis, and is confirmed by our two-level model calculations.

Carbon suboxide is a linear molecule in the ground electronic state. If the dissociating molecule is linear, then, it may be expected that the CO product may not be rotationally excited during the dissociation. This type of result was seen in the dissociations of H_2S and CS_2,[70,71] where SH formed by the dissociation of H_2S was rotationally very cold and CS formed by the dissociation of CS_2 was rotationally very hot. These results were interpreted as showing that the dissociative states of H_2S and CS_2 are linear and bent, respectively. We have investigated this possibility by using an "impulsive" model[9–11] as formulated by Tuck,[12] and by Dugan and Anthony[14] to predict the vibrational, rotational, and translational energy release to the CO product. The impulsive model assumes that the available energy is initially released to the products as kinetic energy to the two atoms that form the dissociating bond. This initial energy release is then partitioned into the fragments translational, rotational, and vibrational degrees of freedom according to the conservation of linear and angular momentum, and the conservation of total energy. The equations used are given below [Eqs. (10)–(13)].

$$E_t^c = [m_c/(m_c + m_c)]E_{av} = 0.50E_{av}, \tag{10}$$

$$E_t^{CO} = (m_c/m_{CO})E_t^c = 0.214E_{av}, \tag{11}$$

$$E_r^{CO} = (m_c/2)(r_c^2 \sin^2\chi/I_{CO})E_{av}, \tag{12}$$

$$E_v^{CO} = E_t^c - E_t^{CO} - E_r^{CO} = (0.50 - 0.214 - 0.285 \sin^2\chi)E_{av}, \tag{13}$$

where E_t^{CO}, E_r^{CO}, and E_v^{CO} are the CO products final translational, rotational, and vibrational energies, r_c is the distance from the CO center of mass to the carbon atom, χ is the CCO bond angle, and I_{CO} is the CO moment of inertia. We fit the observed rotational distributions by varying the equilibrium CCO bond angle, χ^0, and assuming a Gaussian distribution of angles about the equilibrium angle, $f(\chi) = \exp[-(\chi - \chi^0)^2/\omega^2]$, where ω is the width of the distribution

TABLE IV. Impulsive model results for energy partitioning to CO in the photodissociation of C_3O_2.[a]

Photolysis wavelength (nm)	C_2O state	χ^0,(°)	ω,(°)	T_v^0(K)	T_r^0(K)
193	$\tilde{X}^3\Sigma^-$	165	15	7755	4335
193	$\tilde{a}^1\Delta$	162.5	17.5	5053	3092
193	$\tilde{A}^3\Pi_i$	159	26	3420	2206
193	$\tilde{b}^1\Sigma^+$	157	22.5	2831	1911
248	$\tilde{X}^3\Sigma^-$	155.5	25.5	3214	2247
248	$\tilde{a}^1\Delta$	143.5	33	760	660

[a] These results were obtained by fitting the experimental rotational distributions.

of angles. The rotational distributions were calculated as the probability of forming CO in a particular J state, $P(J)$, given by $P(J) = f[\chi(J)]\Delta\chi(J)$, where $\Delta\chi(J)$ is given by $\chi(J+1) - \chi(J)$, and $\chi(J)$ is calculated by inverting Eq. (12). It is possible to qualitatively fit the observed rotational distributions with this model by adjusting the value and width of the equilibrium bond angle. The results of these calculations for possible electronic states of C_2O at both photolysis wavelengths are given in Table IV.

The impulsive model results for the 193 nm photodissociation of carbon suboxide agree with the experimental observations if the dissociating carbon suboxide molecule has a CCO bond angle of $\sim 149°$, and C_2O is formed in the $\tilde{b}\,^1\Sigma^+$ electronic state. The model cannot fit the experimentally observed results for a linear dissociation geometry. The results for the 248 nm photodissociation of carbon suboxide are not in agreement with the experimentally observed results for either possible electronic state of C_2O.

The impulsive model has some shortcomings associated with it. The predicted rotational distributions are non-Boltzmann whereas the experimentally measured rotational distributions are well described by Boltzmann distributions. The model cannot predict vibrational energy distributions or translational energies for particular CO quantum states. Rather, it only predicts the average vibrational energy and the average translational energy. Additionally, the *ad hoc* assumption of a nonlinear CCO bond angle may not be correct. Carbon suboxide does have a very low frequency bending vibration ($\nu_7 \sim 20$ cm^{-1}), however, this vibration is a bend of the CCC bond angle not the CCO bond angle. *Ab initio* calculations by Walch[38] and Osamura *et al.*[72] indicate that the CCO bond angle in carbon suboxide should be nominally 0°. Impulsive models have been shown to best fit experimental energy disposal results when the dissociation occurs directly (i.e., on a repulsive surface).[9-11,70,71] In the case of carbon suboxide photodissociation, the best evidence points to a predissociative fragmentation.

The statistical and impulsive models described cannot completely account for the photodissociation dynamics of carbon suboxide. The microcanonical model successfully describes the vibrational and translational energy release to the Co fragment, but fails to account for the rotational energy release. This result suggests that there may be some nonstatistical dynamical constraint on rotational energy release during the dissociation of carbon suboxide. C_2O has a very low frequency bending mode, and it may be possible that this bending mode can effectively couple with the developing free rotations of the C_2O and CO fragment. If this occurred, C_2O could act as a rotational energy sink, reducing the rotational excitation of the CO fragment. The LIF spectra of C_2O produced from the photodissociation of carbon suboxide shows a large amount of rovibrational excitation in the C_2O fragment.[44] We cannot rule out the possibility of a non-Boltzman rotational distribution. Our experiment measured only the J levels up to $J = 30$, and we cannot rule out the possibility of a secondary maximum in J which could account for the temporal behavior in T_r. However, the results of McFarlane *et al.*[39] also indicate a monotonic decrease in rotational population with increasing J, supporting our results.

It is possible that there is more than one channel for dissociation open at either wavelength. If several channels were open, the observed CO distributions would represent a linear combination of distributions from each active channel. However, there is no clear evidence for this, such as a bimodal rotational distribution or the direct observation of multiple C_2O states by other investigators. Therefore we have assumed that carbon suboxide dissociates to CO and C_2O by a single channel at both wavelengths.

In the above calculations we have assumed that there are no exit channel barriers to the production of electronically excited C_2O. The thermal recombination of CO and C_2O to form carbon suboxide proceeds without a significant barrier; so in the absence of any evidence to support them, we do not postulate *a priori* the existence of exit channel barriers. If there are indeed exit channel barriers to dissociation, then the height and shape of the barriers would have to be considered in any theoretical calculations (see Ref. 35). In terms of our calculations, exit channel barriers would reduce the theoretical energy distributions and possibly shift some of the energy from vibrations to rotations and translations, depending upon the shape of the exit side of the barrier.

The experimental and theoretical results for the photodissociation of carbon suboxide suggest that at 193 nm carbon suboxide dissociates to form C_2O in a state of singlet multiplicity. This result is consistent with the results of Bauer *et al.*[49] and Yamada *et al.*[50] who observed no direct production of C_2O in the $\tilde{A}\,^3\Pi_i$ or $\tilde{X}\,^3\Sigma^-$ states. For photolysis at 248 nm, the results of the present study suggest that carbon suboxide dissociates to form ground state $C_2O(\tilde{X}\,^3\Sigma^-)$, consistent with the results of other investiga-

tors.[44–46,48] We propose, based upon the results of our statistical model, that upon photolysis at 193 nm carbon suboxide dissociates to form $C_2O(\tilde{a}^1\Delta)$ and that the 248 nm photolysis of carbon suboxide yields $C_2O(\tilde{X}^3\Sigma^-)$ as the major product.

V. CONCLUSIONS

The vibrational, rotational, and translational energy released to the CO photofragment produced in the 193 and 248 nm photodissociation of carbon suboxide has been measured using time-resolved infrared absorption spectroscopy. The primary products of the photolysis of carbon suboxide at these wavelengths are C_2O and CO. The nascent CO vibrational distributions can be characterized by effective vibrational temperatures: $T_v^0(193\text{ nm}) = 3030 \pm 49$ K and $T_v^0(248\text{ nm}) = 2070 \pm 22$ K. The average translational energy of various $CO(v,J)$ states was measured by collecting transient absorption spectra at different frequency positions across the absorption line shape. We have also measured the rotational distributions in CO vibrational levels $v = 0 - 2$. The results obtained for the rotational distributions indicate that the method of infrared absorption spectroscopy may suffer from what we call translational and rotational aliasing effects. Nevertheless, using the results obtained, we can estimate the nascent rotational temperatures which characterize the rotational distributions.

The experimental results obtained can not be simply fit using an impulsive model for dissociation, unless assumption of a nonlinear dissociation geometry or multiple dissociation channels are made. Available evidence does not require such assumptions. A statistical model that we have developed to describe energy partitioning in polyatomic photodissociation reactions can reproduce the experimentally measured CO vibrational distributions and average translational energy release at both 193 and 248 nm. This model however, fails to account for the rotational energy release at either photolysis wavelength. The observed rotational distributions are much "colder" than the model predicts. We propose that there may be some dynamical constraint on rotational energy release, possibly a rotational–vibrational coupling in the C_2O fragment which acts as a rotational energy sink during the dissociation process.

Using the results of our statistical model, we propose that the most likely products of carbon suboxide photodissociation at 193 and 248 nm are $CO(X^1\Sigma^+)$ and $C_2O(\tilde{a}^1\Delta)$, and $CO(X^1\Sigma^+)$ and $C_2O(\tilde{X}^3\Sigma^-)$, respectively. Additionally, our experimental and theoretical results indicate that "quasilinear" molecules[73] such as carbon suboxide may have dynamical constraints that exclude rotational excitation of one of the fragments upon dissociation.

[1] S. R. Leone, Adv. Chem. Phys. **50**, 255 (1982).
[2] S. R. Leone, Acc. Chem. Res. **16**, 88 (1983).
[3] F. F. Crim, Annu. Rev. Phys. Chem. **35**, 657 (1984).
[4] K. P. Lawley (Ed.), Adv. Chem. Phys. **60**, (1985).
[5] W. M. Jackson and H. Okabe, Adv. Photochem. **13**, 1 (1986).
[6] *Molecular Photodissociation*, edited by M. N. R. Ashford and J. E. Baggott (Royal Society of Chemistry, London, 1987).
[7] R. Schinke, Annu. Rev. Phys. Chem. **39**, 39 (1988).
[8] G. E. Hall and P. L. Houston, Annu. Rev. Phys. Chem. **40**, 375 (1989).
[9] G. E. Bush and K. R. Wilson, J. Chem. Phys. **56**, 3626 (1972).
[10] G. E. Bush and K. R. Wilson, J. Chem. Phys. **56**, 3638 (1972).
[11] G. E. Bush and K. R. Wilson, J. Chem. Phys. **56**, 3655 (1972).
[12] A. F. Tuck, Faraday Discuss. **73**, 689 (1977).
[13] R. D. Levine and J. L. Kinsey, in *Atom Molecule Collision Theory*, edited by R. B. Bernstein (Plenum, New York, 1984), p. 693.
[14] C. H. Dugan and D. Anthony, J. Phys. Chem. **91**, 3929 (1987).
[15] P. Pechukas and J. C. Light, J. Chem. Phys. **42**, 3281 (1965).
[16] C. E. Klots, J. Phys. Chem. **75**, 1526 (1971).
[17] M. Quack and J. Troe, Ber. Bunsenges. Phys. Chem. **78**, 240 (1974).
[18] M. Quack and J. Troe, Ber. Bunsenges. Phys. Chem. **79**, 170 (1975).
[19] M. Quack and J. Troe, Ber. Bunsenges, Phys. Chem. **79**, 469 (1975).
[20] R. Schinke and V. Engel, Faraday Discuss. Chem. Soc. **82**, 111 (1986).
[21] C. Wittig, I. Nadler, H. Resiler, J. Catanzarite, and G. Radhakrrishann, J. Chem. Phys. **83**, 5581 (1985).
[22] D. M. Wardlaw and R. A. Marcus, Adv. Chem. Phys. **70**, 231 (1988).
[23] S. J. Klippenstein and R. A. Marcus, J. Chem. Phys. **91**, 2280 (1989).
[24] V. Z. Kresin and W. A. Lester, Jr., Adv. Photochem. **13**, 95 (1986).
[25] P. Andresen, U. Beushausen, D. Häusler, and H. W. Lülf, J. Chem. Phys. **83**, 2548 (1985).
[26] D. Häusler, P. Andresen, and R. Schinke, J. Chem. Phys. **87**, 3949 (1987).
[27] D. G. Truhlar, *Potential Energy Surfaces and Dynamics Calculations for Chemical Reactions and Molecular Energy Transfer* (Plenum, New York, 1981).
[28] E. Heller, Acc. Chem. Res. **14**, 368 (1981).
[29] K. Weide, S. Henning, and R. Schinke, J. Chem. Phys. **91**, 7630 (1989).
[30] M. Nonella, J. R. Huber, A. Untch, and R. Schinke, J. Chem. Phys. **91**, 194 (1989).
[31] I. C. Chen, W. H. Green, and C. B. Moore, J. Chem. Phys. **89**, 314 (1988).
[32] C. X. W. Qian, M. Noble, I. Nadler, H. Reisler, and C. Wittig, J. Chem. Phys. **83**, 5573 (1985).
[33] M. Nodle, C. X. W. Qian, H. Reisler, and C. Wittig, J. Chem. Phys. **84**, 3573 (1986).
[34] J. P. Holland and R. N. Rosenfeld, Chem. Phys. Lett. **145**, 481 (1988).
[35] J. P. Holland and R. N. Rosenfeld, J. Chem. Phys. **89**, 7217 (1988).
[36] H. Okabe, *Photochemistry of Small Molecules* (Wiley, New York, 1978), pp. 319–323.
[37] S. W. Bensen, *Thermochemical Kinetics* (Wiley, New York, 1976).
[38] S. P. Walch, J. Chem. Phys. **72**, 5679 (1980).
[39] J. McFarlane, J. C. Polanyi, J. G. Shapter, and J. M. Williamson, J. Photochem. Photobio. A **46**, 139 (1989).
[40] M. E. Jacox, D. E. Milligan, N. G. Moll, and W. E. Thompson, J. Chem. Phys. **43**, 3734 (1965).
[41] C. Devillers and D. A. Ramsay, Can. J. Phys. **49**, 2839 (1971).
[42] K. D. Bayes, J. Am. Chem. Soc. **84**, 4077 (1962).
[43] K. D. Bayes, J. Am. Chem. Soc. **85**, 1730 (1963).
[44] V. M. Donnelley, W. M. Pitts, and J. R. McDonald, Chem. Phys. **49**, 289 (1980).
[45] W. M. Pitts, V. M. Donnelley, and A. P. Baronavski, and J. R. McDonald, Chem. Phys. **61**, 451 (1981).
[46] W. M. Pitts, V. M. Donnelley, and A. P. Baronavski, and J. R. McDonald, Chem. Phys. **61**, 465 (1981).
[47] D. G. Williamson and K. D. Bayes, J. Am. Chem. Soc. **90**, 1957 (1968).
[48] K. H. Becker, O. Horie, V. H. Schmidt, and P. Wiesen, Chem. Phys. Lett. **90**, 64 (1982).
[49] W. Bauer, R. Meuser, and K. H. Becker, J. Photochem. **24**, 99 (1984).
[50] C. Yamada, H. Kanamori, H. Horiguchi, S. Tsuchiya, and E. Hirota, J. Chem. Phys. **84**, 2573 (1986).
[51] B. R. Weiner and R. N. Rosenfeld, J. Am. Chem. Soc. **90**, 4037 (1986).
[52] G. Guelachvili and K. N. Rao, *Handbook of Infrared Standards* (Academic, Orlando, 1986).
[53] D. A. Long, F. S. Murfin, and R. L. Williams, Proc. R. Soc. London Ser. A **223**, 251 (1954).
[54] F. A. Miller and W. G. Fately, Spectrochim. Acta **20**, 253 (1964).
[55] D. J. Miller and R. C. Millikan, J. Chem. Phys. **53**, 3385 (1970).
[56] J. C. Stephenson and E. R. Mosburg, Jr., J. Chem. Phys. **60**, 3562 (1974).
[57] D. F. Starr, J. K. Hancock, and W. H. Green, J. Chem. Phys. **61**, 5421 (1974).
[58] J. T. Yardley, *Introduction to Molecular Energy Transfer* (Academic, New York, 1980).
[59] R. Loudon, *The Quantum Theory of Light* (Claredon, Oxford, 1983), pp. 59–78.
[60] R. L. Roebber, J. Chem. Phys. **54**, 4001 (1971).
[61] T. Minato, Y. Osamura, S. Yamabe, and K. Fukui, J. Am. Chem. Soc.

102, 581 (1980).
[62]E. N. Karyakin, A. F. Krupnov, and S. M. Shapin, J. Mol. Spectrosc. **94**, 283 (1982).
[63]J. Jortner, S. A. Rice, and R. M. Hocstrasser, Adv. Photochem. **7**, 149 (1969).
[64]J. L. Kinsey, J. Chem. Phys. **54**, 1206 (1971).
[65]D. Bogan and D. W. Setser, J. Chem. Phys. **64**, 586 (1976).
[66]D. J. Bamford, S. V. Filseth, M. F. Foltz, J. W. Hepburn, and C. B. Moore, J. Chem. Phys. **82**, 3032 (1985).
[67]J. D. Goddard and H. F. Schaefer III, J. Chem. Phys. **70**, 5117 (1979).
[68]D. Debarre, M. Lefebvre, M. Péalat, J. P. E. Taran, D. J. Bamford, and C. B. Moore, J. Chem. Phys. **83**, 4476 (1985).
[69]The two-level model that we have used calculates the observed P branch absorption signal, S_J, as the difference in the actual populations between the lower and upper states, $n_J^1 - n_{J-1}^2$. The time-dependent population of state "a" is given by $n_J^a(t) = f_v^a(2J+1)\exp[-BJ(J+1)/kT_r^a(t)]$, where B is the CO rotational constant, f_v^a is the fractional vibrational population in level a, k is Boltzmann's constant, and $T_r^a(t)$ is the rotational temperature of level a. $T_r^a(t)$ was determined from an exponential fit of the rotational temperature versus delay time data; $T_r^a(t) = 300 + T_r^a(t=0)\exp(-k_a t)$.
[70]W. G. Hawkins and P. L. Houston, J. Chem. Phys. **76**, 729 (1982).
[71]S. C. Yang, A. Freedman, M. Kawasaki, and R. Bersohn, J. Chem. Phys. **72**, 4058 (1980).
[72]Y. Osamura and K. Nishimoto, Theor. Chim. Acta **52**, 257 (1979).
[73]Quasilinear molecules are linear molecules that have very low frequency bending vibrations. For example, see M. Winnewisser, J. Mol. Struct. **126**, 41 (1985).